

2-D waveguide power transfer operating at 6.78 MHz with a meander surface sheet

Yuichi Masuda
*Department of Complexity
 Science and Engineering
 The University of Tokyo*
 Chiba, Japan
 masuda@hapis.k.u-
 tokyo.ac.jp

Yoshiaki Hirano
TEIJIN LIMITED
 Tokyo, Japan
 yo.hirano@teijin.co.jp

Tsuyoto Negishi
TEIJIN LIMITED
 Tokyo, Japan
 ts.negishi@teijin.co.jp

Hiroyuki Shinoda
*Department of Complexity
 Science and Engineering
 The University of Tokyo*
 Chiba, Japan
 hiroyuki_shinoda@k.u-
 tokyo.ac.jp

Abstract— We propose a new sheet-like waveguide structure for long-range 2-D waveguide power transfer (2DWPT). To achieve the low-loss propagation of electromagnetic (EM) wave guided by the sheet, we try to reduce the operating frequency from 2.4 GHz to 6.78 MHz while maintaining sufficient EM coupling between the sheet and a special coupler. The propagation loss, transmission efficiency and specific absorption rate (SAR), which determine the upper limit of the power supply, are verified by full-wave simulation. The simulated results show that 39.4% efficiency is possible with -0.1 dB/m propagation loss. In addition, 6.6 kW or 660 W can be safely supplied in the case that a person stands upright or lies on the sheet, respectively.

Keywords—2-D waveguide, proximity coupling, SAR, energy confining structure, wireless power transmission (WPT)

I. INTRODUCTION

In this paper, we propose a long-range 2-D waveguide power transfer (2DWPT) by using a sheet-like waveguide medium that has a meander-shaped conductor pattern on its surface (Fig. 1). Because the wavelength in the meander surface sheet is drastically shortened, a 6.78 MHz industrial, scientific, and medical (ISM) band can be used in the proposed 2DWPT. The transmission range is extended to 10 m or more while maintaining practical transmission efficiency.

Wireless power transfer (WPT) is classified as follows: one is the long-range remote WPT, the other one is close-range proximity WPT. The microwave beam [1,2] or magnetic resonance [3,4] are used in the former system. While sufficient transmission distance and efficiency can be achieved, strong electromagnetic (EM) fields are generated between the transmitter and receiver.

The later system can confine the most EM fields around a transmission waveguide medium and receiver although the freedom in the receiver position is limited to 1-D or 2-D plane. An electric vehicle on electric roadway (EVER) system [5,6], which is one of the solutions of the close-range proximity WPT, can achieve the long-range and safety WPT. Capacitive coupling between a power transmission line buried under the road and a wheel-type coupler is used. The strong electric field concentrates in the tire rubber.

2DWPT is another solution to the close-range proximity WPT. In the 2DWPT, the EM wave propagates in the sheet-like waveguide medium while generating an evanescent field on its surface. A special coupler, which couple with the evanescent field, extract the EM power from the sheet. And it has the freedom of the position on the 2-D plane with a small air-gap [7,8].

Most of the EM energy is confined in the sheet or the gap between sheet and coupler. Sufficient specific absorption rate (SAR) and electromagnetic interference (EMI) can be achieved because of the physical isolation of these regions.

In the previous 2DWPT, a desk mat-sized waveguide sheet was used with the 2.4 GHz ISM band. If the operation frequency reduces, the propagation loss in the sheet will reduce and the transmission range will extend. On the other hand, the coupling coefficient between sheet and coupler will reduce.

In this work, we solve this trade-off by changing the sheet surface conductor pattern. The rest of this paper is organized as follows. In Section II, the structure of the proposed meander surface sheet is explained. Section III shows the simulated results. The propagation loss, transmission efficiency, and SAR are verified. Finally, Section IV concludes this paper.

II. MEANDER SURFACE SHEET

This section shows the structure of the meander surface sheet and describes the trade-off between the transmission efficiency and the propagation loss.

A. Structure of the meander surface sheet

The structure of the meander surface sheet is shown in Fig. 1. The EM wave propagates in the dielectric layer sandwiched between a ground conductor and a meander-shaped conductor. The meander-shaped conductor slows down the propagation speed of the current that flows in the direction of the EM wave propagation (X-direction). Thus, the wavelength in the sheet is shortened as the current meanders.

B. Tradeoff between the Efficiency and Propagation Loss

The intensity of the evanescent field can be controlled by sheet surface reactance X_0 denoted as follows:

$$X_0 = \frac{\omega((1/\kappa c)^2 - \mu_s \epsilon_s)}{\epsilon_s / h}, \quad \kappa = \lambda_s / \lambda \quad (1)$$

where c , λ , λ_s and κ , are the speed of light, wavelength in vacuum, wavelength in a sheet, and wavelength shortening rate, respectively. (1) shows that a high coupling coefficient

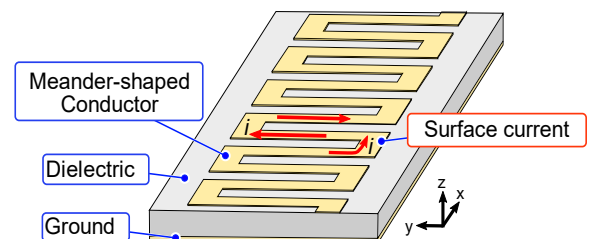


Fig. 1 Wavelength-shortening sheet with a meander-shaped conductor pattern. The meandering current slows the propagation speed of EM waves in the X-direction. Thus, the wavelengths of the EM waves propagating in the X-direction are shortened.

between sheet and coupler can be achieved by shortening the wavelength.

Here, we define the power in the sheet at distance x from power source, P_{IN} , as follows:

$$P_{IN} = P_{SUP} \exp(-2\alpha x) \quad (2)$$

where P_{SUP} and α represents the power supply and the attenuation constant denoted as follows:

$$\alpha = \frac{\pi}{\lambda_s} \tan\delta + \frac{R_0}{2h\sqrt{\mu_s/\epsilon_s}} \quad (3)$$

where $\tan\delta$ and R_0 are loss tangent of the dielectric layer and the sheet surface resistance. (2) and (3) show that the propagation loss can be reduced at the low operating frequency in terms of λ_s and R_0 .

According to (1) and (3), sufficient sheet reactance can be achieved even at the operating frequency if the wavelength is strongly shortened.

Table 1 shows the specifications of the meander surface sheet and a capacitive coupler in consideration of the trade-off. And the cross-sectional views of the sheet and coupler and their parameters are shown in Fig. 2.

Table 1 : Specifications

Sym-bol	Description	value	Sym-bol	Description	value
ω	angular frequency [rad/s]	$2\pi \cdot 6.78 \cdot 10^6$	$X2$	meander line spacing 2 [m]	0.1
h	sheet thickness [m]	0.01	$Y1$	Y-direction meander length [m]	0.46
μ_s	sheet permeability [H/m]	$1.26 \cdot 10^{-6}$	W	meander line width [m]	0.01
ϵ_s	sheet permittivity [F/m]	$2.1 \cdot 8.85 \cdot 10^{-12}$	L_{cp}	X-direction coupler length [m]	0.75
$X1$	meander line spacing 1 [m]	0.04	d	Z-direction coupler distance [m]	0.03

III. FULL WAVE SIMULATION

This section shows the propagation loss, transmission efficiency, and SAR by using the full-wave simulation model based on Table. 1.

A. Propagation Loss and EM field

Fig. 3 shows the simulation model of the meander surface sheet. The $\pm x$ end of the sheet is the input port (Port1) and the output port (Port2) respectively. The propagation loss is calculated by using the simulated S-parameter and (4). The length of the sheet in the x-direction is 1 m.

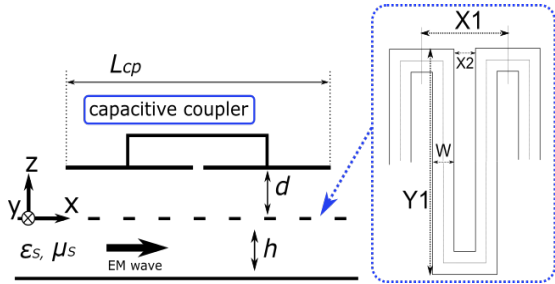


Fig. 2 Cross-sectional views of the sheet and coupler and their parameters.

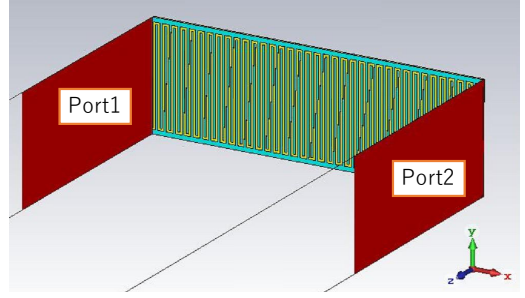


Fig. 3 Simulation model of the meander surface sheet. $H=0$ boundary in the $\pm y$ direction and OPEN boundary in the other direction.

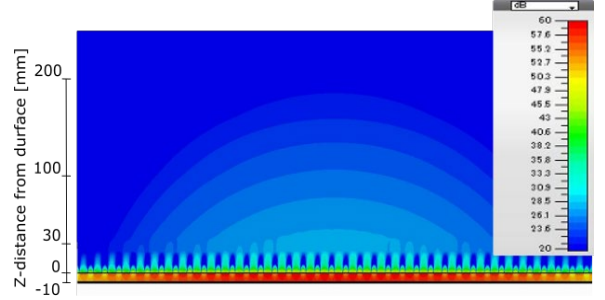


Fig. 4 . Absolute value of the electric field in the Z direction in the X-Z plane at the center of the sheet.

$$PropLoss = 10 \log_{10} \left(\frac{|S_{21}|^2}{1 - |S_{11}|^2} \right) \quad (4)$$

The calculated result of the propagation loss is shown in Table 2.

Table 2: Calculated result of the propagation loss

Description	value
propagation loss [dB/m]	-0.104309

The absolute value of the electric field in the Z direction in the X-Z plane at the center of the sheet is shown in Fig. 4. Even at 6.78 MHz, a part of the EM wave leaks out to the surface of the sheet, as in the conventional waveguide sheets.

B. Efficiency with Electric field coupler

The simulation model of the sheet and the capacitive coupler, based on the specifications in Table 1, is shown in Fig. 5. The simulated results of the S-parameter are shown in Fig. 6.

Table 3 shows the transmission efficiency η obtained based on (5). The S-parameter at 6.78 MHz is used.

$$\eta = 10 \log_{10} \left(\frac{|S_{31}|^2}{1 - |S_{11}|^2} \right) \quad (5)$$

Table 3: Calculated transmission efficiency

Description	value
efficiency [dB]	-4.04

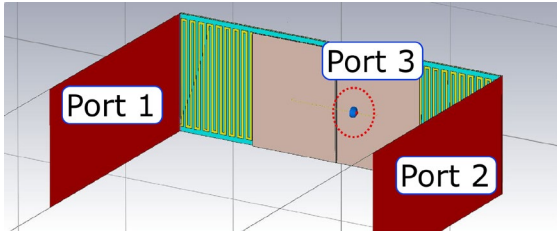


Fig. 5 Simulation model of the sheet and the capacitive coupler, based on the specifications in Table 1. The two electrodes are connected to the coupler output (Port 3: Discrete Port) via a conductor line. A coil element is connected in series between the output section and the conductor to resonate at 6.78 MHz.

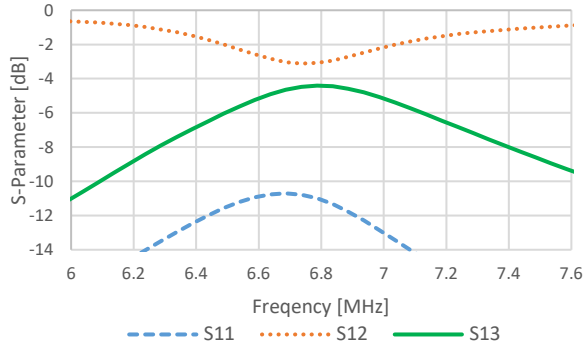


Fig. 6 Simulated results of the S-parameters.

The coupler output (S_{31} [dB]) is maximized at 6.78 MHz, which is the resonance frequency. The efficiency is -4.04 dB (about 39.4 % in percentage terms).

Note that the maximum efficiency of this model is -3 dB. If a signal enters the coupler, it branches to both ends of the sheet. It means that $S_{13} = S_{23}$ because of the symmetry of this model. Thus, the maximum S_{31} is -3 dB since $S_{13} = S_{31}$.

C. SAR

The SAR is a measure of the rate at which energy is absorbed per unit mass by a human body when exposed to the EM field. Local SAR is the time average over a small sample volume (typically 1 g or 10 g of tissue). According to the ICNIRP guidelines, the upper limit of the local SAR in the limbs is 4 W/kg [9].

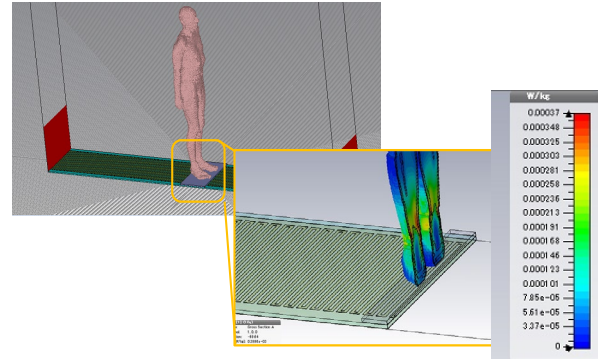
The local SAR was evaluated by using the human models that place in the upright and supine positions (Fig. 7). The maximum power supply is calculated from (5). The maximum SAR shown in Fig 5 is used.

$$\text{maximum power supply} = P_{IN} \times (4/\text{maximum SAR}) \quad (6)$$

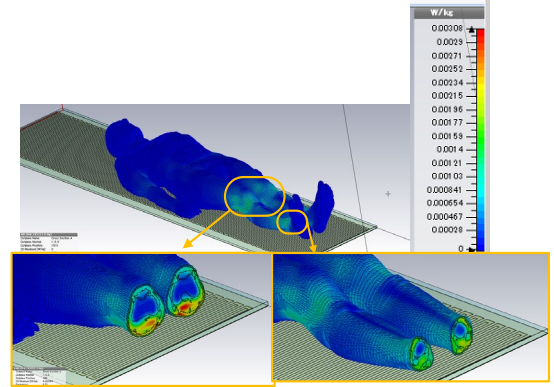
Table. 4 shows that 6.6 kW and 660 W can supply when the human models place in the upright and supine positions, respectively.

Table 4: Maximum power supply at each state (6.78 MHz)

State	P_{IN} [W]	Maximum SAR [W/kg]	Maximum power supply [W]
upright	0.5	0.000303	6600
supine	0.5	0.00308	660



(a)



(b)

Fig. 7 SAR of the human models that place in the upright and supine positions (a) SAR value with the upright position model at 1 cm above the sheet (b) SAR value with the supine position model at 1 cm above the sheet. The operating frequency is 6.78 MHz.

Fig. 8 shows the maximum coupler output at each position from the power source. The results shown in Table 2-4 are used. And the maximum power supply in the case of the upright state is used.

While keeping the safety, more than 1.5 kW of power can be supplied to the loads connected to the coupler over a distance of 20 m. In this case, about 2.0 kW of the remaining power, which is not extracted by the coupler, can be recovered at the termination of the 20m sheet.

IV. CONCLUSION

In this paper, a meander surface sheet was proposed to extend the transmission distance of 2DWPT. The feasibility of a long-range 2DWPT system was verified based on three-dimensional full-wave simulations. The operating frequency

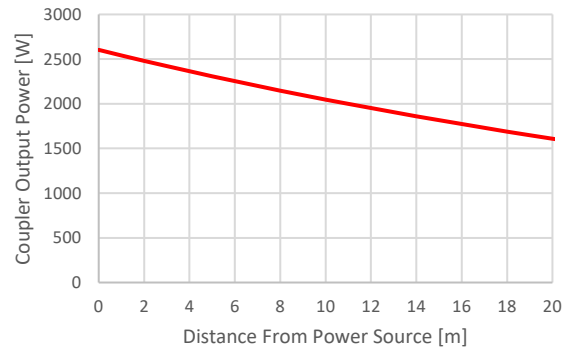


Fig. 8 Calculated results in an upright position. Coupler output power vs the distance from the power source.

was reduced from 2.4 GHz to 6.78 MHz, and a propagation loss of -0.1 dB/m, and a transmission efficiency of -4.04 dB was observed.

From the SAR value obtained by the pseudo-human model, the meander surface sheet can be supplied up to 6.6 kW EM power while maintaining the safety standards. Even with the human body placed on the supine positions, which was considered the most dangerous, the upper limit was 660 W.

REFERENCES

- [1] B. Yang, X. Chen, J. Chu, T. Mitani, and N. Shinohara, "A 5.8-GHz Phased Array System Using Power-Variable Phase-Controlled Magnetrons for Wireless Power Transfer," *IEEE Transactions on Microwave Theory and Techniques*, pp. 1–1, 2020, doi: 10.1109/TMTT.2020.3007187.
- [2] N. Takabayashi, N. Shinohara, T. Mitani, M. Furukawa, and T. Fujiwara, "Rectification Improvement With Flat-Topped Beams on 2.45-GHz Rectenna Arrays," *IEEE Transactions on Microwave Theory and Techniques*, vol. 68, no. 3, pp. 1151–1163, Mar. 2020, doi: 10.1109/TMTT.2019.2951098.
- [3] H. Kim et al., "Coil Design and Measurements of Automotive Magnetic Resonant Wireless Charging System for High-Efficiency and Low Magnetic Field Leakage," *IEEE Transactions on Microwave Theory and Techniques*, vol. 64, no. 2, pp. 383–400, Feb. 2016, doi: 10.1109/TMTT.2015.2513394.
- [4] P. Machura and Q. Li, "A critical review on wireless charging for electric vehicles," *Renewable and Sustainable Energy Reviews*, vol. 104, pp. 209–234, Apr. 2019, doi: 10.1016/j.rser.2019.01.027.
- [5] T. Ohira, "A battery-less electric roadway vehicle runs for the first time in the world," in 2017 IEEE MTT-S International Conference on Microwaves for Intelligent Mobility (ICMIM), Mar. 2017, pp. 75–78, doi: 10.1109/ICMIM.2017.7918860.
- [6] S. Sakihara, S. Kitabayashi, N. Sakai, and T. Ohira, "Far-End Reactor Matching to a Traveling Load Along an RF Power Transmission Line," *IEICE Transactions on Fundamentals of Electronics, Communications and Computer Sciences*, vol. E101.A, no. 2, pp. 396–401, 2018, doi: 10.1587/transfun.E101.A.396.
- [7] H. Shinoda, Y. Makino, N. Yamahira, and H. Itai, "Surface Sensor Network Using Inductive Signal Transmission Layer," *Proc. Fourth International Conference on Networked Sensing Systems*, pp. 201–206, July 2007, doi: 10.1109/INSS.2007.4297420.
- [8] A. Noda and H. Shinoda, "Selective Wireless Power Transmission Through High-Q Flat Waveguide-Ring Resonator on 2-D Waveguide Sheet," *IEEE Transactions on Microwave Theory and Techniques*, vol. 59, no. 8, pp. 2158–2167, Aug. 2011, doi: 10.1109/TMTT.2011.2156425.
- [9] International Commission on Non-Ionizing Radiation Protection, "ICNIRP GUIDELINES", Vol. *Health Physics* 99, no. 6, pp. 818–836, 2010.